J. theor. Biol. (1977) **67**, 11–24

A Hydrodynamical Model of Bordered Pits in Conifer Tracheids

D. C. CHAPMAN†, R. H. RAND‡ AND J. R. COOKE§

Cornell University, Ithaca, New York 14853, *U.S.A.*

(*Received* 24 *March* 1976, *and in revised form* 6 *August* 1976)

Bordered pits are small structures in the cell walls of tracheid xylem cells in plants. Coniferous bordered pits are typified by a closing membrane possessing a torus and margo structure. This paper presents a hydrodynamical model which supports the conjecture that coniferous bordered pits act like valves to fluid flowing in the xylem pathway.

By means of an approximate solution and a corresponding stability analysis, the model is shown to permit only flows with flow rates smaller than a certain critical flow rate Q^*. Flow rates larger than Q^* are shown to be associated with an unstable equilibrium configuration. As a result of this instability, the pit "snaps" shut and stops the flow.

1. Introduction

BORDERED PITS IN CONIFER TRACHEIDS

Tracheids are xylem cells which provide a major pathway for the flow of water from the roots of a plant to its transpiring leaves, especially in conifers. Pits are small structures in the cell walls of tracheids which permit water to flow from one tracheid to an adjoining tracheid (Keeton, 1967; Esau, 1965).

A typical coniferous bordered pit consists of a circular border which arches over the pit cavity and contains a closing membrane. The closing membrane is made up of a thick central region called the torus and a thin peripheral region called the margo (i.e. edge or margin) [Fig. 1(a)] (Liese, 1965; Schmid, 1965; Tsoumis, 1965). The torus is relatively impermeable to the flow of water while the margo is perforated and therefore relatively permeable to water.

† Graduate Student, Department of Agricultural Engineering.
‡ Associate Professor, Department of Theoretical and Applied Mechanics.
§ Associate Professor, Department of Agricultural Engineering.

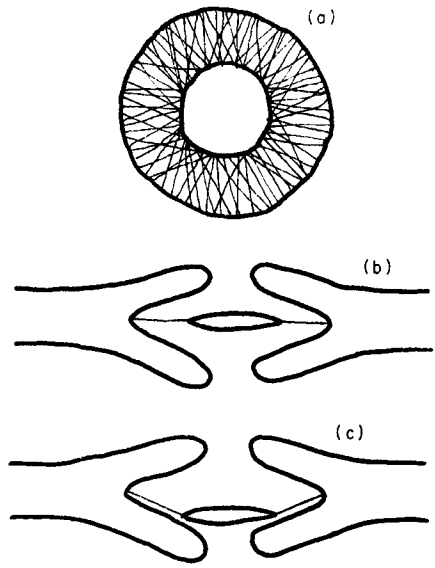

FIG. 1. Bordered pits. (a) The closing membrane is made up of a thick central region (the torus) and a thin peripheral region (the margo). (b) The border (porus) arches over the pit cavity and contains the closing membrane, shown unaspirated (open). (c) Same pit shown aspirated (closed).

The border of a bordered pit, called the porus, consists of secondary wall material which has separated from the middle lamella (the middle lamella is a thin layer which lies between the walls of adjacent cells) (Bailey, 1913; Fengel, 1972; Mia & Chauret, 1972). A typical bordered pit has two pori, one in each tracheid [Fig. 1(b)].

The bordered pit is found in nature both in unaspirated (open) [Fig. 1(b)] and in aspirated (closed) states [Fig. 1(c)] (Petty, 1972; Gregory & Petty, 1973). In the unaspirated state water can flow from one tracheid to the other through the margo. In the aspirated state the torus is pressed firmly against the porus and virtually no flow occurs through the pit.

It has been conjectured in the literature that the bordered pit acts like a valve controlling the fluid flowing through it (Bailey, 1913; Fengel, 1972; Hammel, 1967; Mark & Crews, 1973; Muhlethaler, 1961). For small flows the pit remains unaspirated and acts like an open valve. For large flows, pressure forces on the torus are believed to cause aspiration, thereby making the pit act like a closed valve. The purpose of this work is to support this hypothesis with an analysis of the mechanics of the bordered pit, and to provide a greater understanding of how the pit closes.

Note that this work applies only to bordered pits with a torus and margo structure. Such pits are typical in conifers but are rare in angiosperms.

2. The Model

We will present a two-dimensional model based upon the geometry of Fig. 2.

The margo is modeled by two linear springs and the torus by a rigid plate constrained to move parallel to its initial position. It is assumed that water flows freely through the margo while the torus acts as an impermeable boundary to the fluid flow. The fluid is assumed to be inviscid and incompressible with constant density. The flow is assumed to be irrotational and steady (Vallentine, 1959).

Laplace's equation is well known to govern the flow of this hydrodynamics problem (Vallentine, 1959). Since the model is two-dimensional, a solution to the fluid flow problem may be sought via the theory of analytic functions of a complex variable.

Once the flow is found, the pressure distribution on the torus will yield the total fluid force on the torus. Equating this fluid force with the restoring force of the springs gives the equilibrium configuration of the pit.

A stability analysis reveals that for a given geometry, fluid density, and spring constant, the pit permits only flows with flow rates smaller than a certain critical flow rate Q^*. Flow rates larger than Q^* are shown to be associated with an unstable equilibrium configuration. As a result of this instability, the pit "snaps" shut and stops the flow.

3. The Hydrodynamics Problem

We present an approximate (but closed form) solution to the two-dimensional hydrodynamics problem of the flow around the torus (Fig. 2).

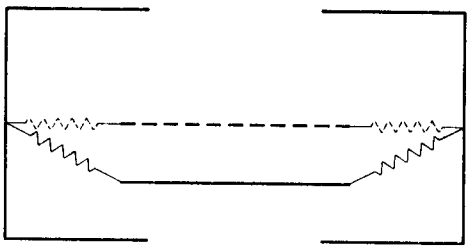

FIG. 2. Geometry of two-dimensional model. Solid lines represent displaced position of torus, dotted lines represent initial position.

Our approximation is motivated by considerations from Bernoulli's equation,

$$\tfrac{1}{2}\rho v^2 + p = \text{constant} \tag{1}$$

where ρ = fluid density,
v = magnitude of fluid velocity vector,
p = fluid pressure.

In an equilibrium configuration in which the torus is displaced towards the lower porus (as in Fig. 2), the fluid speed v is larger near the lower side of the torus than near the upper side of the torus. (In an incompressible fluid, conservation of mass requires that v must increase where the width of the flow decreases.) Then from Bernoulli's equation the pressure on the lower side of the torus is smaller than the pressure on the upper side of the torus. There results a net fluid force downward which opposes the elastic forces of the margo.

In order to model this effect in a mathematically tractable manner we consider the flow between two overlapping semi-infinite plates (Fig. 3). We shall approximate the force of the fluid on the torus of Fig. 2 by first calculating the force of the fluid on the plates of Fig. 3 and then superimposing Fig. 3 four times to approximate the four torus–porus (plate–wall) interactions of Fig. 2 (see Fig. 4).

FIG. 3. Two semi-infinite overlapping plates. Compare with Fig. 4.

The validity of this approximation has been verified by finite difference numerical integration of Laplace's equation with boundary conditions corresponding to Fig. 2. This will be discussed later.

We calculate the force of the fluid on the plates of Fig. 3 by use of conformal mapping. By a handbook transformation (Kober, 1957) of the theory of complex variables, the overlapping semi-infinite plates of the complex z-plane are mapped to the real axis of the complex t-plane (see Fig. 5).

The transformation has the form

$$z = t + \frac{b}{t} + 2c \ln t \tag{2}$$

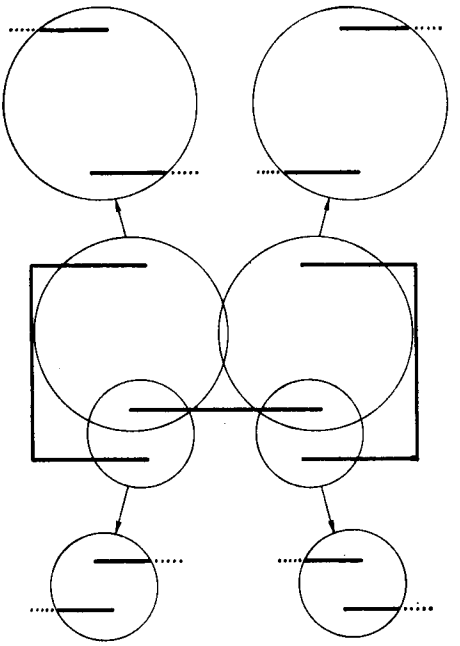

FIG. 4. The semi-infinite overlapping plates of Fig. 3 are superimposed four times to approximate the four torus-porus (plate-wall) interactions of the model. See text.

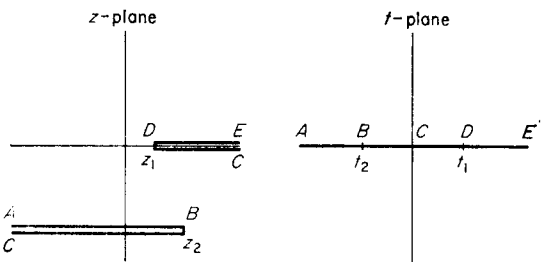

FIG. 5. Equation (2) maps the overlapping semi-infinite plates in the complex z-plane to the real axis in the complex t-plane. Note that the plates have zero thickness.

where $b > 0$, $c < 0$ are real constants which determine the distance between the plates $[= 2\pi|c| = \mathrm{Im}\,(z_1 - z_2)]$ and the plate overlap distance $[= \mathrm{Re}\,(z_2 - z_1)]$. The tips of the plates z_1, z_2 map to the points t_1, t_2 respectively, where

$$\begin{aligned} t_1 &= -c + \sqrt{b + c^2} \\ t_2 &= -c - \sqrt{b + c^2}. \end{aligned} \tag{3}$$

Note that the plates have zero thickness.

To obtain a flow in the t-plane which corresponds to a downward flow in the z-plane between the plates, we place a sink at the origin in the t-plane. This corresponds to the complex potential (Vallentine, 1959)

$$w = -\frac{Q}{\pi} \ln t \tag{4}$$

where Q is the flow rate. Here

$$\frac{\mathrm{d}w}{\mathrm{d}z} = \left(\frac{\mathrm{d}w}{\mathrm{d}t} \Big/ \frac{\mathrm{d}z}{\mathrm{d}t}\right)$$

is the complex velocity in the z-plane.

The downward force, F, of the fluid on the plate located on the real z axis ($y = 0$) is

$$F = \int_{z_1}^{\infty} \Delta p \, \mathrm{d}z \tag{5}$$

where $\Delta p = p(y = 0^+) - p(y = 0^-)$.

Using Bernoulli's equation (1) with $v^2 = |\mathrm{d}w/\mathrm{d}z|^2$, p may be eliminated from equation (5). The resulting integral is evaluated in the Appendix, with the outcome

$$F = \frac{\rho Q^2}{4\pi^2} \frac{1}{\sqrt{b + c^2}} \ln \left|\frac{t_1}{t_2}\right| \tag{6}$$

where t_1, t_2 are given in terms of b and c by equations (3).

The total force of the fluid F_f on the torus of Fig. 4 is found by using equation (6) four times. Let

δ = displacement of the torus from its undisplaced position (midway between the pori),

h = torus–porus overlap distance,

L = distance between pori (i.e. pit's depth).

Then $F_f = 2F_1 - 2F_2$, where F_1 and F_2 are F of equation (6) with $L/2 - \delta$ and $L/2 + \delta$ taken as the distance between plates ($= 2\pi|c|$), respectively.

The resulting expression for F_f may be written in the form

$$F_f = \frac{\rho Q^2}{h} f\left(\frac{\delta}{h}; \frac{L}{h}\right). \tag{7}$$

Here L/h is viewed as a non-dimensional geometric parameter, fixed for a given pit. The non-dimensional quantity δ/h represents the torus displacement, variable for a given pit.

The force F_f is displayed in Fig. 6. Note that $F_f \to \infty$ as $\delta \to L/2$ (aspiration) and that the slope of the F_f curve is strictly positive for $\delta = 0$. Also shown in Fig. 6 is the resulting F_f found by finite difference numerical integration of Laplace's equation for the geometry shown in Fig. 7. Figure 7 also shows a typical flow pattern (Chapman, 1976).

Comparison of the curves in Fig. 6 shows identical qualitative behavior and limited quantitative agreement between the approximate closed form solution (7) and the approximate finite difference numerical solution.

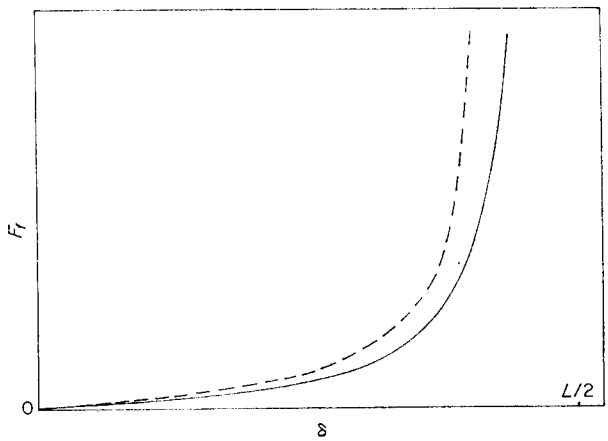

FIG. 6. The total force of the fluid on the torus, F_f, displayed as a function of the torus displacement, δ, for the geometry of Fig. 7. Solid line represents approximate closed form solution, dotted line represents approximate finite difference numerical solution.

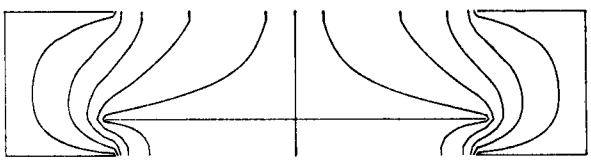

FIG. 7. Streamlines for flow around torus from approximate finite difference numerical solution.

4. Equilibrium

At equilibrium, the force of the fluid on the torus, F_f, is equal and opposite to the elastic restoring force, F_e, of the margo on the torus. The margo is modeled as two linearly elastic springs which are unstretched when the torus is midway between the pori (i.e. when $\delta = 0$).

If λ represents the unstretched spring length and if each spring has spring constant $\kappa/2$, then (Fig. 8)

$$F_e = 2 \sin\theta \left[\frac{\kappa}{2}(\sqrt{\lambda^2+\delta^2}-\lambda)\right]$$
$$F_e = \kappa\delta\left\{1-\left[1+\left(\frac{\delta}{\lambda}\right)^2\right]^{-\frac{1}{2}}\right\}. \tag{8}$$

The force F_e is displayed in Fig. 8. Note that the slope of the F_e curve is zero for $\delta = 0$.

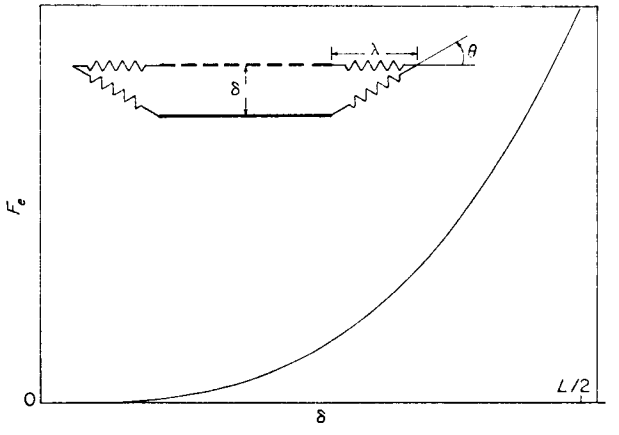

FIG. 8. The elastic restoring force, F_e, of the margo (modeled as springs) on the torus, displayed as a function of the torus displacement δ.

Equating F_f [equation (7), Fig. 6] with F_e for equilibrium yields the equilibrium displacement δ as a function of the other model parameters. Figure 9 shows a non-dimensional plot of $\rho Q^2/\kappa h^2$ versus δ/h for fixed values of L/h and λ/h (geometrical parameters).

For a given geometry, fluid density and spring constant, a flow rate Q determines up to three equilibrium values of δ. The displacement $\delta = 0$ is (by symmetry) always an equilibrium configuration. It will be shown to be unstable and hence physically unrealizable except if $Q = 0$. If Q is

sufficiently small ($Q < Q^*$, Fig. 9) then two other equilibrium values of δ exist. Their stability will be discussed next. For values of $Q > Q^*$ the only equilibrium displacement is $\delta = 0$. It will be shown that such values of Q correspond to the closed valve behavior of the pit.

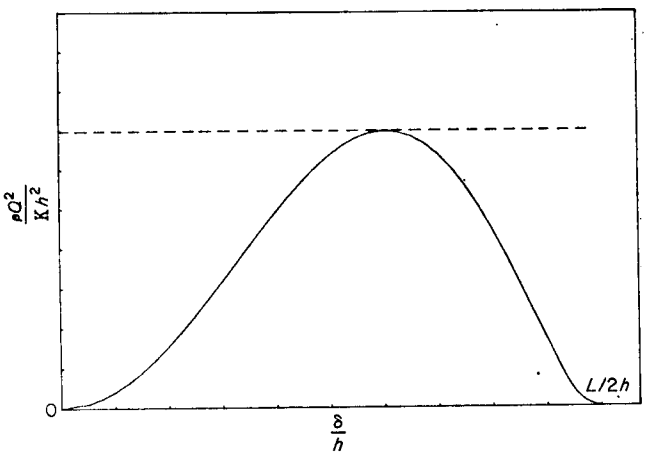

FIG. 9. Equilibrium torus displacements. The dotted line corresponds to $Q = Q^*$ (for fixed parameters ρ, κ, h, L, λ).

5. Stability of Equilibrium

An equilibrium configuration $\delta = \bar{\delta}$ will be called stable if an infinitesimally small perturbation produces a motion $\delta = \delta(\tau)$ which remains close to the equilibrium $\delta = \bar{\delta}$ for all time $\tau \geq 0$. An equilibrium configuration which is not stable is said to be unstable.

In order to consider the motions of the torus about an equilibrium position, we will require the equation of motion of the torus. Neglecting the inertia of the fluid compared to that of the torus, Newton's Second Law for the torus becomes

$$m\ddot{\delta} = F_f - F_e = \Phi(\delta) \tag{9}$$

where m = mass of the torus,

$$\Phi(\delta) = F_f - F_e = \text{net force on the torus,}$$

and where dots represent differentiation with respect to time τ.

Figure 10 displays $\Phi(\delta)$ for the three cases $Q < Q^*$, $Q = Q^*$ and $Q > Q^*$, for typical values of the model parameters (compare with Figs 6 and 8).

Expanding $\Phi(\delta)$ in a Taylor Series about an equilibrium position $\delta = \bar{\delta}$,

$$\Phi(\delta) = \Phi(\bar{\delta}) + \Phi'(\bar{\delta}).(\delta - \bar{\delta}) + \ldots \tag{10}$$

where primes represent differentiation with respect to δ. At a point of equilibrium $\Phi(\bar{\delta}) = 0$. Substituting equation (10) into equation (9) and linearizing,

$$m\ddot{\xi} - \Phi'(\bar{\delta})\xi = 0 \tag{11}$$

where $\xi = \delta - \bar{\delta}$ = displacement from the equilibrium position $\delta = \bar{\delta}$ and where

$$\Phi'(\bar{\delta}) = \text{slope of } \Phi(\delta) \text{ at } \delta = \bar{\delta} \text{ (Fig. 10).}$$

The solutions to equation (11) are bounded for all $\tau \geq 0$ if and only if $\Phi'(\bar{\delta}) < 0$. Therefore the condition for $\delta = \bar{\delta}$ to be a stable equilibrium configuration is $\Phi'(\bar{\delta}) < 0$. From Fig. 10, $\delta = 0$ is always unstable (unless $Q = 0$). For $Q < Q^*$ there are two additional equilibria. In this case the equilibrium position corresponding to the smaller value of δ is stable while the other equilibrium is unstable.

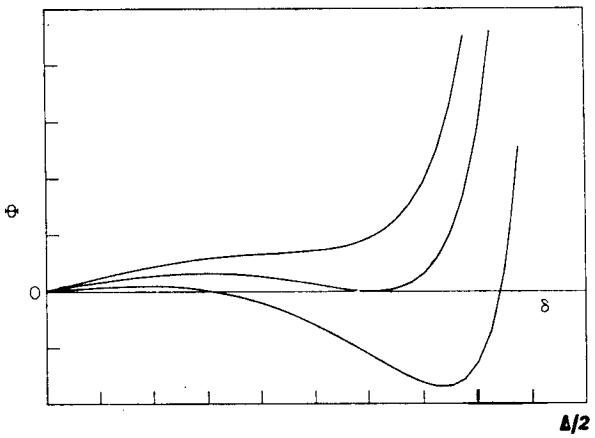

FIG. 10. The net force on the torus, Φ, displayed as a function of δ. The upper, middle and lower curves correspond respectively to $Q > Q^*$, $Q = Q^*$ and $Q < Q^*$.

Suppose now that $Q < Q^*$ and that the pit is in its stable equilibrium configuration. As Q is gradually (quasi-statically) increased to a value just below Q^*, the torus correspondingly advances to a new (but still stable) equilibrium position. Since the fluid is incompressible, all the fluid that enters through one pit aperture leaves through the other and the pit acts like an open valve to the fluid flow.

As Q is increased to a value just above Q^*, the previously stable equilibrium position coalesces with the previously unstable equilibrium position and both disappear. For $Q > Q^*$ the force on the torus $\Phi(\delta)$ is strictly positive

for $0 < \delta \leq L/2$ (Fig. 10). The torus responds to the increase in Q beyond Q^* by increasing δ [in accordance with equation (9)] until $\delta = L/2$, i.e. until the torus comes in contact with the porus. The pit has snapped shut.

The pit may then be held closed by hydrostatic forces or by surface tension (Petty, 1972). Alternately, a chattering effect could be predicted for the pit: when the pit closes the fluid ceases to flow and F_f, the force holding the torus closed, goes to zero. Then the torus, acted upon by F_e, begins to open. As soon as the torus moves away from the porus, the fluid begins to flow again and F_f, no longer zero, snaps the pit shut once more, etc.

6. Extensions of the Model

The effects of viscosity and of the third dimension on the model have been investigated by finite difference numerical integration of the Navier–Stokes equations for the axisymmetric geometry of Fig. 11 (Chapman, 1976). The resulting relationship between the fluid force on the torus, F_f, and the torus displacement, δ, is shown in Fig. 12.

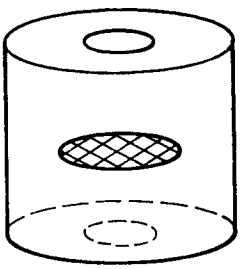

FIG. 11. Geometry of three dimensional axisymmetric viscous fluid model (Chapman, 1976).

It has been found that in the presence of viscosity the flow must be accompanied by a pressure drop across the pit. (This effect is similar to the pressure drop encountered in Poiseuille pipe flow.) Moreover, $\delta = 0$ is no longer found to be an equilibrium position: the presence of viscous drag forces on the torus eliminate the symmetry which caused the $\delta = 0$ configuration to be an equilibrium position in the inviscid model. This corresponds in Fig. 12 to F_f being non-zero when $\delta = 0$.

Although the three-dimensional viscous model gives values of F_f which are substantially larger than those of the two-dimensional inviscid model (with unit depth in the third dimension) presented above, both models behave qualitatively the same.

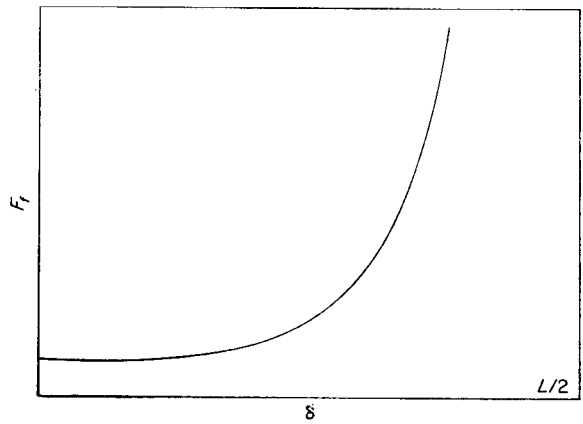

FIG. 12. The total force of the fluid on the torus, F_f, displayed as a function of the torus displacement, δ, for the three dimensional axisymmetric viscous fluid model of Fig. 11. Note that F_f is non-zero when $\delta = 0$. Note also that this figure is not drawn to the same vertical scale as the corresponding two dimensional inviscid plot, Fig. 6. In fact the three dimensional viscous model predicts values of F_f which are substantially larger than those of the two dimensional inviscid model (with unit depth in the third dimension).

7. Conclusion

The mathematical model of coniferous bordered pits presented in this paper has been shown to support the conjecture that such pits act like valves to fluid flow. Specifically, moderate flows are permitted to pass relatively unimpeded, while large flows are prevented.

REFERENCES

BAILEY, I. W. (1913). Reprinted in *Contributions to Plant Anatomy* (1954), p. 207. Waltham, Mass.: Chronica Bot. Co.

CHAPMAN, D. C. (1976). A Mathematical Analysis of Bordered Pits in Tracheids, M.S. thesis in Dept. of Agricultural Engineering, Cornell University, Ithaca, N.Y.

ESAU, K. (1965). *Plant Anatomy*, 2nd edn. New York: Wiley.

FENGEL, D. (1972). *Holzforschung*. **26**, 1.

GREGORY, S. C. & PETTY, J. A. (1973). *J. exp. Botany* **24**, 763.

HAMMEL, H. T. (1967). In *Proceedings of the Spring* 1967 *Colloquia on the Interactions Between Engineering and the Biological and Agricultural Sciences*, sponsored by Biological Engineering Programs, University of Mass., Amherst, Mass.

KEETON, W. T. (1967). *Biological Science*. New York: Norton.

KOBER, H. (1957). *Dictionary of Conformal Representations*. New York: Dover.

LIESE, W. (1965). In *Cellular Ultrastructure of Woody Plants* (W. A. Cote, ed.). Syracuse, N.Y.: Syracuse U. Press.

MARK, W. R. & CREWS, D. L. (1973). *For. Sci.* **19**, 241.

MIA, A. J. & CHAURET, G. (1972). *Tex. J. Sci.* **24**, 293.

MUHLETHALER, K. (1961). In *The Cell*, vol. II (J. Brachet & A. E. Mirsky, eds), p. 85. New York: Academic Press.

PETTY, J. A. (1972). *Proc. R. Soc. Lond. B*, **181**, 395.
SCHMID, R. (1965). In *Cellular Ultrastructure of Woody Plants* (W. A. Cote, ed.), p. 291. Syracuse, N.Y.: Syracuse U. Press.
TSOUMIS, G. (1965). In *Cellular Ultrastructure of Woody Plants* (W. A. Cote, ed.), p. 305. Syracuse, N.Y.: Syracuse U. Press.
VALLENTINE, H. R. (1959). *Applied Hydrodynamics*. London: Butterworths.

Appendix

We derive equation (6) from equation (5) as follows:

$$F = \int_{z_1}^{\infty} \Delta p \, dz = \int_{\substack{z_1 \\ \text{on } y=0^+}}^{\infty} p \, dz - \int_{\substack{z_1 \\ \text{on } y=0^-}}^{\infty} p \, dz$$

$$= \int_{\substack{\infty \\ \text{on } y=0^-}}^{z_1} p \, dz + \int_{\substack{z_1 \\ \text{on } y=0^+}}^{\infty} p \, dz = \int_{\substack{0 \\ t \text{ real}}}^{\infty} p \frac{dz}{dt} \, dt.$$

From Bernoulli's equation (1) with $v^2 = |dw/dz|^2$,

$$p = -\tfrac{1}{2}\rho \left|\frac{dw}{dz}\right|^2 + \text{constant}.$$

On the plate $y = 0$, the velocity dw/dz is real. Hence

$$\left|\frac{dw}{dz}\right|^2 = \left(\frac{dw}{dz}\right)^2 = \left(\frac{dw}{dt}\right)^2 \Big/ \left(\frac{dz}{dt}\right)^2$$

and

$$F = -\tfrac{1}{2}\rho \int_0^{\infty} \left[\left(\frac{dw}{dt}\right)^2 \Big/ \frac{dz}{dt}\right] dt.$$

(The constant term in p can be ignored since it contributes nothing to Δp.)
Now from equations (2) and (4),

$$\frac{dz}{dt} = 1 - \frac{b}{t^2} + \frac{2c}{t}$$

$$\frac{dw}{dt} = -\frac{Q}{\pi t}$$

and

$$F = -\frac{\rho Q^2}{2\pi^2} \int_0^{\infty} \frac{dt}{t^2 + 2ct - b}.$$

Although this is a standard indefinite integral,

$$\int \frac{\mathrm{d}t}{t^2+2ct-b} = \frac{1}{2\sqrt{b+c^2}} \ln \left| \frac{t+c-\sqrt{b+c^2}}{t+c+\sqrt{b+c^2}} \right|$$
$$= \frac{1}{2\sqrt{b+c^2}} \ln \left| \frac{t-t_1}{t-t_2} \right|,$$

the denominator of the integrand vanishes at $t = t_1$ (corresponding to infinite velocities and pressures at the plate tip $z = z_1$). Taking the Cauchy principal value,

$$F = -\frac{\rho Q^2}{2\pi^2} \lim_{\varepsilon \to 0} \left\{ \int_0^{t_1-\varepsilon} \frac{\mathrm{d}t}{t^2+2ct-b} + \int_{t_1+\varepsilon}^{\infty} \frac{\mathrm{d}t}{t^2+2ct-b} \right\}$$

$$F = \frac{\rho Q^2}{4\pi^2} \frac{1}{\sqrt{b+c^2}} \ln \left| \frac{t_1}{t_2} \right|.$$